Journal Pre-proofs

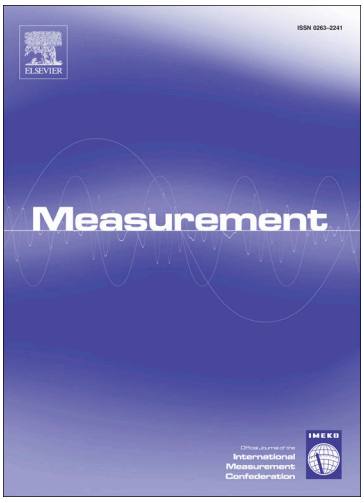

Freeform surface adaptive interferometry assisted with simulated annealing-hill climbing algorithm

Lei Zhang, Renhu Liu, Jinling Wu, Zhongtao Cheng, Sheng Zhou, Jingsong Li, Benli Yu

PII: S0263-2241(21)00571-6
DOI: https://doi.org/10.1016/j.measurement.2021.109597
Reference: MEASUR 109597

To appear in: *Measurement*

Received Date: 27 September 2020
Revised Date: 5 May 2021
Accepted Date: 12 May 2021

Please cite this article as: L. Zhang, R. Liu, J. Wu, Z. Cheng, S. Zhou, J. Li, B. Yu, Freeform surface adaptive interferometry assisted with simulated annealing-hill climbing algorithm, *Measurement* (2021), doi: https://doi.org/10.1016/j.measurement.2021.109597

Freeform surface adaptive interferometry assisted with simulated annealing-hill climbing algorithm

Lei Zhang[a,c,*], Renhu Liu[a,c], Jinling Wu[a,c], Zhongtao Cheng[b], Sheng Zhou[a,c], Jingsong Li[c], Benli Yu[a,c]

[a] *Information Materials and Intelligent Sensing Laboratory of Anhui Province, Anhui University, Hefei, 230601, China*

[b] *Division of Engineering and Applied Science, California Institute of Technology, 1200 E. California Blvd., Pasadena, California 91125, USA*

[c] *Key Laboratory of Opto-electronic Information Acquisition and Manipulation Ministry of Education, Anhui University, Hefei, 230601, China*

ARTICLE INFO

Keywords:
Freeform surface
Adaptive interferometer
Simulated annealing
Hill climbing

ABSTRACT

The freeform surface adaptive interferometer (FSAI) recently has been employed to realize the unknown freeform surface metrology. A near null interferogram should be acquired from the initial interferogram with undistinguished fringes even dark areas. The direct optimization object in FSAI is just the interferogram rather than the focusing intensity characterization in traditional wavefront-sensorless (WFS) adaptive systems. The simulated annealing-hill climbing (SA-HC) mixed algorithm is employed in the FSAI, which has much better convergence than the stochastic parallel gradient descent (SPGD) algorithm, almost as much as the genetic algorithm (GA). At the same time, it is much faster than GA and thus applicable to the test of volume-produced in the optical shop. Simulations and experiments validating the algorithm feasibility are presented.

1. Introduction

Optical freeform surfaces have great application potential on request by miniaturization of optical systems [1-3]. Due to its freedom of generating aberrations, system performance will also be improved accordingly. Just because of freedom, its surface metrology is always being challenged [4]. Interferometry, playing an important role in the high precision test of flat, spherical, and aspheric surfaces [5-7], has got attention in freeform surface metrology as well. The aberration compensator becomes the first thing to be considered in a freeform surface interferometer. However, several null [8, 9] and non-null compensators [10, 11] in aspheric interferometry seem powerless in freeform surface interferometry because they can only afford rotational symmetric aberrations. The only one left available is the computer-generated hologram (CGH) [12], which is designed to generate a special wavefront for matching the tested surface. However, the specially designed CGH can only accommodate a unique tested surface, which costs much in the optical shop test. Moreover, the CGH design is impossible for an unknown tested surface form, which happens a lot in the state of freeform surface fabrication. In the fabrication process, the freeform surface is revised constantly [13], which makes all the above static compensators useless. A programmable dynamic compensator is required to cover the unknown surface in fabrication. Several dynamic compensators have been developed, in which adaptive optics, such as the deformable mirror (DM) and liquid crystal spatial light modulator (LC-SLM), have the most prominent performance. The freeform surface adaptive interferometer (FSAI) thus has been proposed [14-23] based on the DM and LC-SLM, aiming to perform adaptive aberration correction to realize the near null test in testing freeform surfaces with various shapes. The near null fringes would be acquired from the initial interferogram with the implementation of the adaptive compensation algorithm. With a tested surface of large departure, there would be indistinguishable fringes even dark areas in the initial interferogram, from which the wavefront phase is unable to be demodulated. That is the FSAI usually works as a wavefront-sensorless (WFL) system [24, 25]. As a WFL system, the adaptive compensation algorithm in FSAI aims to provide the optimal control signal of adaptive optics to seek near null fringes without direct aberration (or phase) information. Most of the traditional adaptive control algorithms in WFL systems are based on focusing intensity distribution evaluation [26-30]. Instead of the focusing intensity distribution evaluation, the dominant optimization object is the interferogram in an FSAI [15, 18-21, 31, 32]. 2016, the

∗ Corresponding author.
E-mail address: optzl@ahu.edu.cn (L. Zhang).

https://doi.org/
####-####/

stochastic parallel gradient descent (SPGD) algorithm has been employed to address this issue for the first time in a DM-based FSAI [15]. Subsequently, this method was proved effective in an LC-SLM-based FSAI [18-20]. 2020, an SPGD and Newton iteration mixed algorithm was introduced to address the problem that the single SPGD algorithm cannot realize the absolute null interferogram in the final step [32]. However, the Monte Carlo simulation showed that the SPGD based algorithm is local optimization prone, and thus leads the interferogram always trapped in indistinguishable fringes [31]. Therefore, the genetic algorithm (GA) is employed in an LC-SLM-based FSAI [31] for more intelligent and Monte Carlo simulations showed a more robust convergence characteristic. However, the GA suffers too many iterations and thus is time-consuming [31]. Even though time is not the main consideration in a common test, the GA is still not applicable to test volume-produce in the optical shop because the time cost is high.

In this paper, we discussed the simulated annealing-hill climbing (SA-HC) mixed algorithm for performing the adaptive control in the FSAI for the first time. It tends to get global optimal interferograms from the indistinguishable interferogram and dark areas. Also, it is time-saving. 90% of the time would be saved compared to the GA. Simulations and experiments show that the SA-HC algorithm is more competent than the SPGD algorithm and GA in the freeform surface test in batch in the workshop.

2. Principle of FSAI

The improved configuration of the FSAI is illustrated in Fig. 1(a). The DM and partial null optics (PNO) [10, 11] act as the combined-compensator in the interferometer. The beam from the interferometer is polarized (p-polarized beam) by a polaroid and travels through the polarized beam splitter (PBS). The p-polarized beam would change to the s-polarized one after the reflection by the DM and round-trip transmission through the adjustable quarter-wave plate (AQWP). Then the s-polarized beam is all reflected by the PBS and transmit through the PNO, and then retrace to the AQWP after reflected by the tested freeform surface (FS). After another reflection by the DM and round-trip transmission through the AQWP, the s-polarized beam is changed to a p-polarized one and retrace to interferometer after transmitting through the PBS and polaroid. Then, an interferogram with indistinguishable fringes and even dark areas is generated in the case of a tested FS with a large departure. The SA-HC algorithm is employed to drive the DM deformation as an adaptive aberration compensator, pursuing the near null fringes. The general interferogram variation is presented in Fig. 1(b). Then, the AQWP is rotated by 45°and the DM deformation is tested by the interferometer. Finally, the phase of the FS test results in Fig. 1(a), i.e., the phase of the final interferogram in Fig. 1(b), and the DM deformation tested in Fig. 1(c) is substituted into the system ray-tracing model to reconstruct the figure map of the tested FS [33].

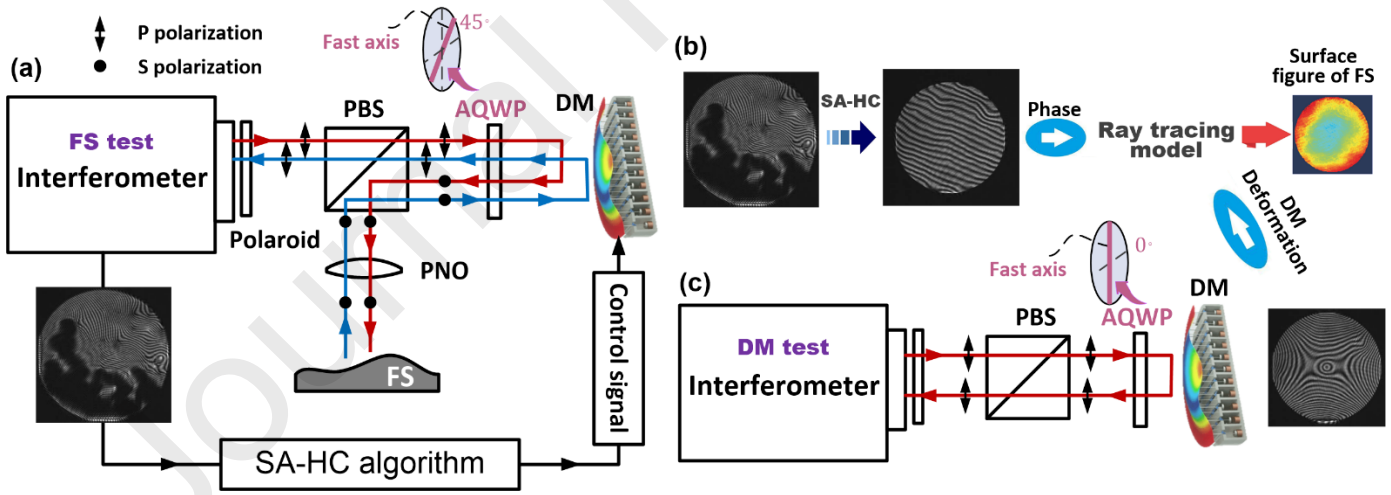

Fig.1. Principle of FSAI. (a)A common configuration of a DM-based FSAI, (b) the interferogram variation, (c) the DM deformation test.

3. SA-HC algorithm in FSAI

We simplify the adaptive control in FSAI into two steps. As is shown in Fig. 2(a), the first one is to recover full aperture distinguishable fringes from the initial interferogram with the dark areas and the undistinguishable fringes. In this step, the SA algorithm is implemented. The second step is to realize the near null fringes from the dense fringes. In this step, the SA algorithm is to work with the aid of the HC algorithm. The specific principle is described below.

3.1 The first step: SA algorithm

The simulated annealing algorithm comes from the process of crystal cooling [34]. If the solid is not in the lowest energy state, the solid is heated and then cooled. As the temperature T drops slowly, the atoms in the solid are arranged in a certain shape to form regular crystals with high density and low energy (min of the energy function), corresponding to the global optimal solution in the algorithm. The essence of the annealing algorithm is to receive the worse cost function value with a certain probability, which simulates the short temperature rise to jump out of the local minimum.

Rather than the sum of squared gray level differences between any two pixels of the interferogram (SSD) [15], the pixel number N_{p} of the dark and indistinguishable area is better to be set as the energy function in FSAI [31]. The first step is calculating the N_{p} in each iterations. The reference[31] calculates the N_{p} with complex machine vision and morphology operation. In this paper, we reconstruct the phase of the interferogram directly as is shown in Fig. 2(a), in which the ineffective area (data missing area) is determined by the dark region and the indistinguishable region of the corresponding interferogram. The calculation of N_{p} is relative accurate.

The N_{p} is directly determined by the voltage vector $\boldsymbol{V}$ of the DM. The iterative change of the $\boldsymbol{V}$ is

$$\boldsymbol{V}_{i+1}^{T(n)} = \boldsymbol{V}_{i}^{T(n)} + \boldsymbol{\gamma}\boldsymbol{V}_{i}^{T(n)} (i = 0 \cdots L), \qquad (1)$$

where $T(n)$ is the temperature of the nth annealing, i means the ith iteration in the L (Markov chain length)[34] iterations at temperature $T(n)$, $\boldsymbol{\gamma}$ is a vector of random number between -1 and 1, refer to the perturbation step length. Thus, the new energy function $N_{\mathrm{p}}(\boldsymbol{V}_{i+1}^{T(n)})$ would be calculated. The change of energy function in each iteration is calculated as

$$\Delta N_{\mathrm{p\_}i+1} = N_{\mathrm{p}}(\boldsymbol{V}_{i+1}^{T(n)}) - N_{\mathrm{p}}(\boldsymbol{V}_{i}^{T(n)}). \qquad (2)$$

The new $\boldsymbol{V}_{i+1}^{T(n)}$ is accepted with a certain probability P, which is called the Metropolis criterion as follows.

$$P(\boldsymbol{V}_{i}^{T(n)} \rightarrow \boldsymbol{V}_{i+1}^{T(n)}) = \begin{cases} 1, & \Delta N_{\mathrm{p\_}i+1} < 0 \\ \exp\left(\frac{\Delta N_{\mathrm{p\_}i+1}}{T(n)}\right), & \Delta N_{\mathrm{p\_}i+1} > 0 \end{cases}. \qquad (3)$$

More clearly, P is determined by

$$P(\boldsymbol{V}_{i}^{T(n)} \rightarrow \boldsymbol{V}_{i+1}^{T(n)}) = \begin{cases} 1, P > Pr \\ 0, P < Pr \end{cases}. \qquad (4)$$

where the random probability $Pr \in [0,1)$.

Whether the new voltage $\boldsymbol{V}_{i+1}^{T(n)}$ is accepted or not, the algorithm will proceed to the next iteration until the $N_{\mathrm{p}}(\boldsymbol{V}_{i+1}^{T(n)}) = 0$ or $i = L$. If $i = L$ and $N_{\mathrm{p}}(\boldsymbol{V}_{i+1}^{T(n)}) \neq 0$, the annealing is performed as

$$T(n+1) = \rho T(n), \ \rho \in (0,1) \qquad (5)$$

Then, the iteration is re-executed at the new temperature $T(n+1)$ until $N_{\mathrm{p}}(\boldsymbol{V}_{i+1}^{T(n+1)}) = 0$.

The whole process can be described as follows. L iterations are performed at each temperature $T(n)$. At each iteration, the new energy function, i.e. the pixel number N_{p} of the dark and indistinguishable area in the interferogram, is calculated according to the new voltage of DM. The new voltage of DM is not always accepted unless the change in energy function satisfies the Metropolis criterion. Whether the new voltage is accepted or not, the algorithm will proceed to the next iteration. An annealing operation begins when the L iterations are completed until the energy function minimizes. At the end of this step, a full aperture interferogram with distinguishable fringes is recovered. The whole process of the SA is illustrated in Fig. 2(b).

3.2 The second step: SA and HC algorithm

Although the full aperture interferogram with distinguishable fringes is recovered, the fringe density is relatively high because the SA in the first step only works for dark area elimination rather than reducing the fringe density of the full aperture. Therefore, the rms value of the interferogram is set as the cost function in the second step to make fringes sparse. Of course, the SA would be effective as well in this step. However, the SA algorithm is not necessary when the fringe density is reduced to a relatively small amount. The HC algorithm with a faster convergence rate would be more competent for the work at this time. Although the HC algorithm is a local search algorithm, whose search result depends on the starting point [35], its search speed is much higher than that of the SA algorithm. With the resulting $\boldsymbol{V}$ acquired in the SA algorithm, the voltage of each actuator of DM (the element in $\boldsymbol{V}$) is changed one by one in this step as follows.

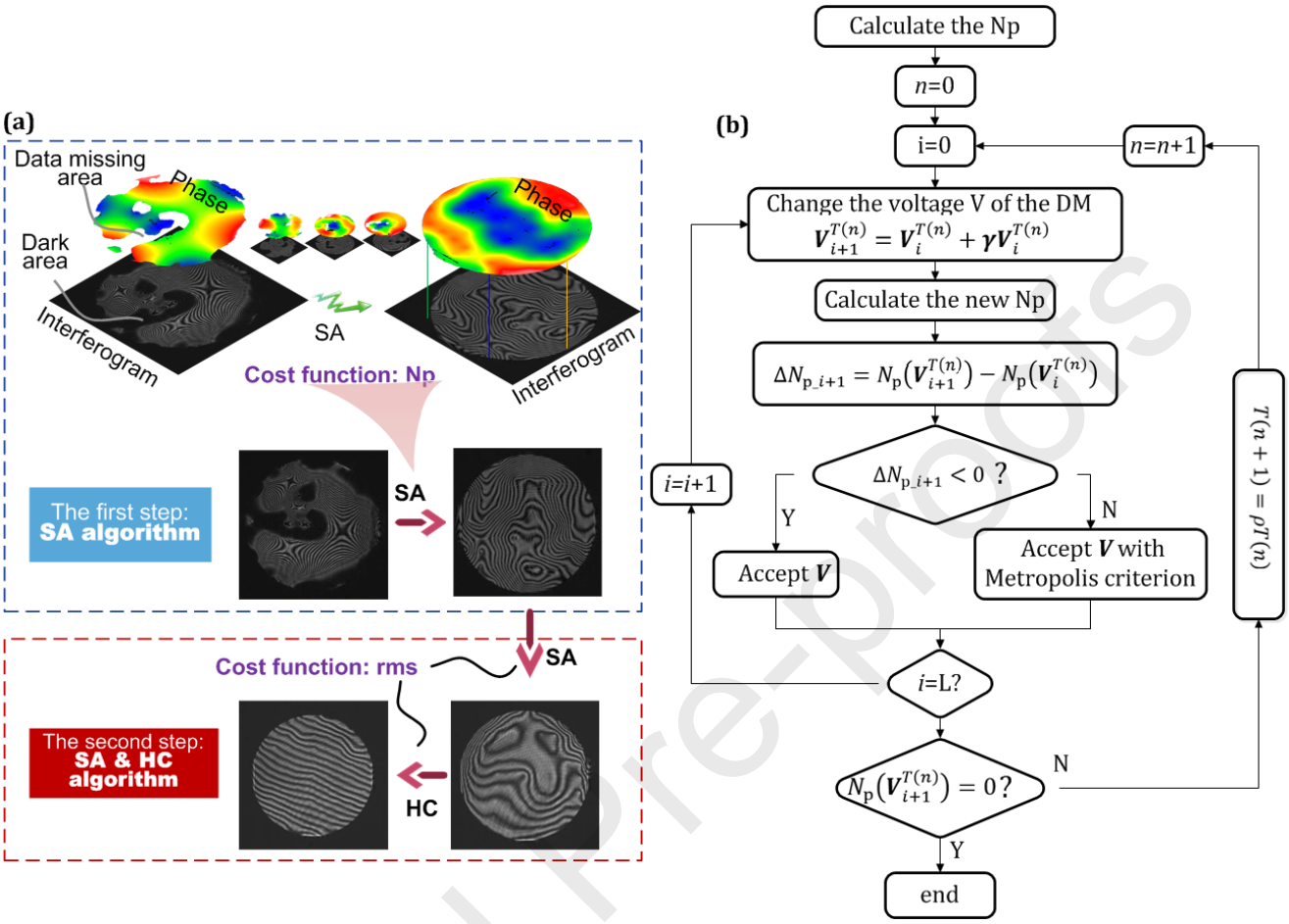

Fig.2. The algorithm flow diagram in FSAI, (a) the whole process, (b) the flow chat the SA algorithm.

$$v(m)_{j+1} = v(m)_j + k_m \Delta v \qquad (6)$$

where, $v(m)$ is the voltage of the mth actuator of the DM, j is the iteration number, and k_m is the voltage disturbance factor. The sign of the k_m is determined by

$$k_m \cdot \Delta \mathrm{rms}_1 < 0 \qquad (7)$$

where, $\Delta \mathrm{rms}_1 = \mathrm{rms}(v(m)_1) - \mathrm{rms}(v(m)_0)$, which is the initial rms variation of the interferogram.

The whole process can be described as follows. The initial voltage of the DM is the end voltage $\boldsymbol{V}$ in the SA algorithm. An actuator voltage of the DM, i.e., an element in $\boldsymbol{V}$, is changed as Eq. (6). Compare the rms value before and after changing to determine the correct direction of the voltage adjustment. If the value of rms decreases, k_m remains unchanged; Otherwise, make $k_m = -k_m$. Then, the voltage is optimized continuously according to the determined k_m until the rms value increases. Finally, perform the above optimization for all actuator voltages.

4. Simulation

Simulations are presented to validate the SA-HC algorithm in the FSAI.

4.1 The first step: SA algorithm

Firstly, we provided a simulation to validate the SA algorithm in the first step of the optimization, aiming to reduce the N_p to zero. The DM in the simulation with 97 actuators has a stroke of about 40 μm, which is the same as the one in the experiment. There are several parameters to be determined in the SA algorithm, such as the initial temperature $T(0)$, Markov chain length L, and the annealing coefficient ρ. Generally, no standard strategy has been developed. The impact of the parameters on the performance of the SA algorithm should be evaluated with consideration of the speed and convergence. Many pieces of research have been made on the optimal parameter selection [36-38]. We provide the determination in FSAI by

experience and simulation. The parameter selection is related to the initial state of the FSAI, i.e. the N_p of the initial interferogram. In our study, the initial temperature $T(0)$ is determined equal to initial N_p. According to [34], ρ is usually chosen between 0.85 and 0.99. In the simulation, the $\rho = 0.92$ provides fine results. The DM control voltages are represented by a 97-element vector $\boldsymbol{V} = [v_1, v_2 \cdots v_{97}]$. On each iteration, v was randomly perturbed by up to 10 % and the new voltages accepted or rejected on the variations of N_p [39]. 30%-40% acceptance rate is considered optimal [40] thus the perturbation size is adjusted by 1/10 of its current value to keep the acceptance rate in the optimal range. An initial interferogram with $N_p \approx 35000$ from the FSAI is selected for optimization as is shown in Fig. 3(a), whose PV is no more than 60 λ. The optimization time is limited in 30 minutes. The GA and SPGD algorithms are implemented for comparison as well. The parameters in the GA and SPGD algorithm are selected as the same in [31]. The gain coefficient in the SPGD is selected as 0.006 and the Δv is 0.04 V. The crossover probability and non-uniform mutation in GA is set as 0.8 and 0.4, respectively. Figures 3(b)-3(d) illustrate the optimization results of the SA algorithm, SPGD algorithm, and GA. The N_p of the three results all go down to zero, which implies the effectiveness of the three algorithms in FSAI. The specific variations of the N_p interactions are presented in Fig. 3 (e). In the three algorithms, the time required to reduce N_p to zero is about 462 s, 267 s, and 1515 s, respectively. The SA algorithm has a much faster convergence rate than GA and slightly less than the SPGD algorithm. Another initial interferogram with $N_p \approx 70000$ from the FSAI is selected for optimization as is

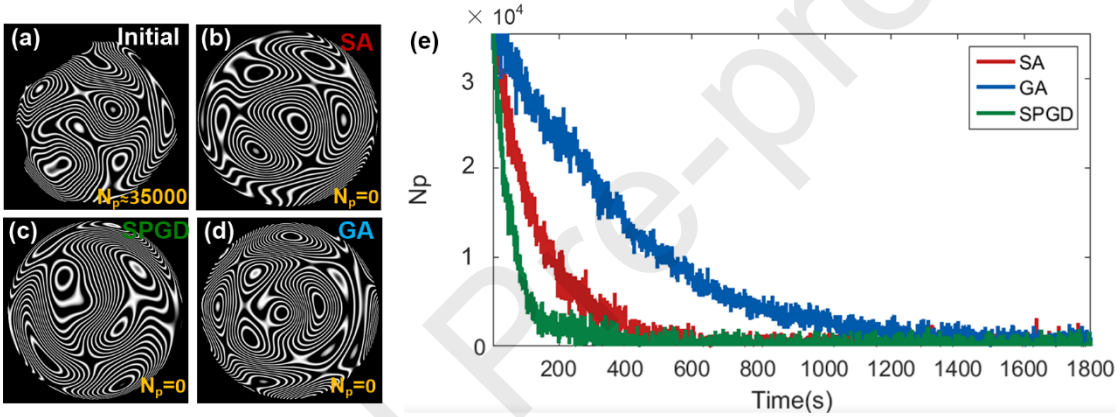

Fig. 3. A simulation example of the SA algorithm in the first step in FSAI, with the comparison with GA and SPGD algorithms. (a) the initial interferogram, (b) the resulting interferogram by the SA algorithm, (c) the resulting interferogram by the SPGD algorithm, (d) the resulting interferogram by the GA.

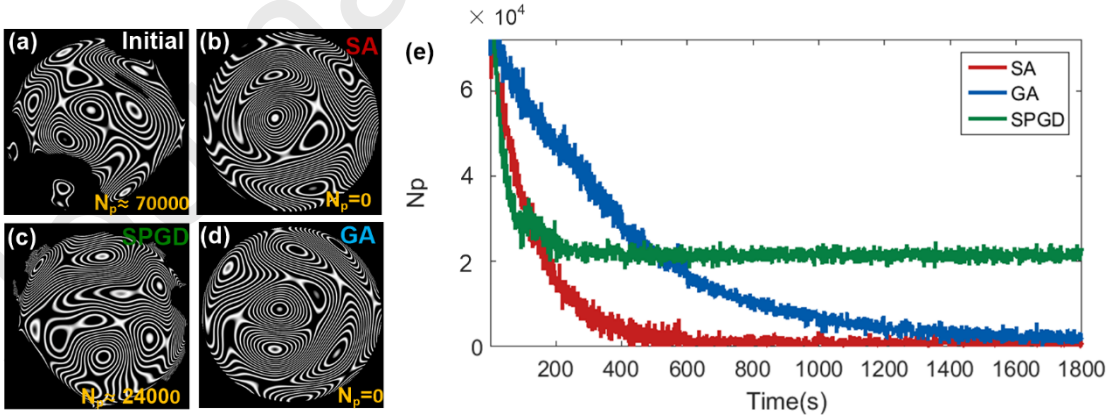

Fig. 4. Another simulation example of the SA algorithm in the first step in FSAI, with the comparison with GA and SPGD algorithms. (a) the initial interferogram, (b) the resulting interferogram by the SA algorithm, (c) the resulting interferogram by the SPGD algorithm, (d) the resulting interferogram by the GA.

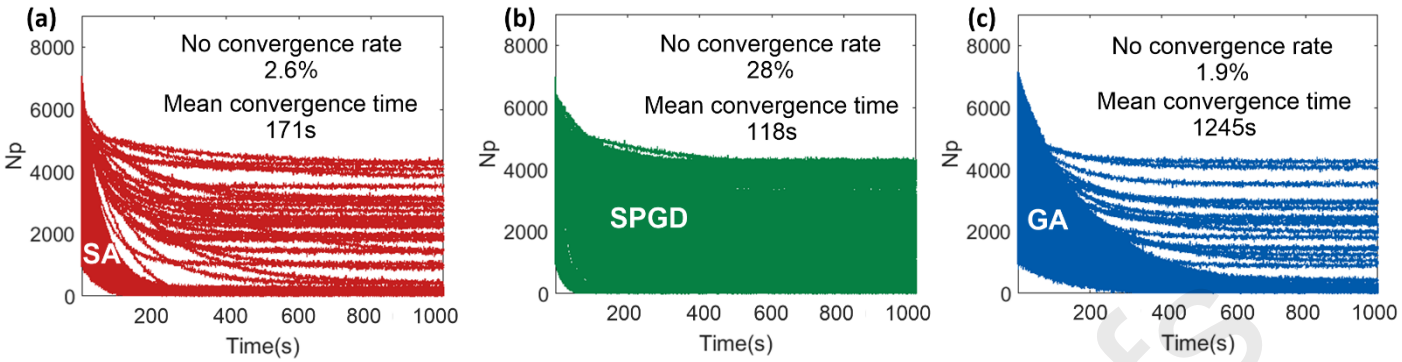

Fig. 5. The Monte Carlo simulation results of the SA algorithm in the first step in FSAI, with the comparison with GA and SPGD algorithms.

shown in Fig. 4(a). Figures 4(b)-4(d) illustrate the optimization results of the SA algorithm, SPGD algorithm, and GA in 30 minutes. The N_{p} results by the SA algorithm and GA go down to zero (Figures 4(b) and 4(d)), while the one by the SPGD algorithm stays around 24000 after 200s. The specific variations of the N_{p} interactions are presented in Fig. 4(e). The SA algorithm and GA still maintain good convergence after 420 s and 1800 s, respectively. However, the SPGD algorithm is stuck in a local minimum after about 200 s.

Therefore, the convergence of these algorithms is worth exploring in FSAI. The Monte Carlo simulations were performed to validate the convergence case of the three algorithms in FSAI. 1000 random interferograms with $1000 < N_{\mathrm{p}} < 10000$ were generated and optimized by the SA, SPGD, and GA in 17 minutes. Figure 5 illustrates the Monte Carlo simulation results, where Figs. 5(a)-5(c) refer to the three algorithms, respectively. The no convergence rate of the SA algorithm is about 2.6%, which is similar to the one of GA (1.9%). The no convergence rate of the SPGD algorithm is about 28%, much higher than that of the SA algorithm and GA. Meanwhile, the mean convergence time of SA, SPGD, and GA is about 171s, 118s, and 1245s, respectively. Obviously, the SA algorithm has much better convergence than the SPGD algorithm in FSAI, almost as much as GA. At the same time, it is much faster than the GA algorithm and thus applicable to the test of volume-produced in the optical shop.

4.2 The second step: SA and HC algorithm

When the first step is completed, the full aperture interferogram with distinguishable fringes is acquired and the second step starts. In the second step, we aim to decrease fringe density to near null and thus the optimization object would be changed to the rms value of the residual fringes. Of course, the SA algorithm would still be effective. The red line in Fig.6 illustrates an example of the rms variations with the increase of the iteration number. The initial rms value in this step is about 8 λ, which refers to a relatively large departure in the polishing stage. The rms decreases to 0.07 λ after about 1600 iterations, which cost about 227 s. We employed the HC algorithm instead of the SA algorithm for optimization when the rms decreased to about 2 λ as the point P shown in Fig. 6, where $k_m = 0.001$. The rms value then dropped quickly and decreased to 0.02λ after about 800 iterations, as the black line shown in Fig. 6 (a). The position of point P plays a decisive role in cost time. The problem is when to perform the HC algorithm. Several interferograms of different initial rms values (rms value of point P) were optimized by the HC algorithm in simulation as is shown in Fig. 6(b). The result shows that the algorithm is no convergence prone when the initial rms value of the interferogram is larger than 4.4λ. That is the HC algorithm is easy to get stuck in local extremes unless there is a good starting point such as a relatively small initial rms value. Therefore, the HC algorithm would be performed when the rms value of the resulting interferogram decreases to about 4 λ in the SA algorithm. Of course, this value is also debatable given the complexity of the form of aberrations.

5. Experiment

Experiments were carried out to validate the SA-HC algorithm in FSAI. The experiment system shown in Fig.7 was set up as Fig. 1. The interferometer is ZYGO Verifire™ of 4'' aperture and the DM is ALPAO 97-25, with the same parameters as in the above simulations. The tested freeform surface was a mechanically pressed reflector of 25mm aperture and a relatively large departure from a flat sheet. Thus, the PNO is not necessary. The CPU employed is the Intel Xeon Scalable 6148. Before the test beginning, the initial interferogram in FSAI was captured by the interferometer. It is shown in the first figure of Fig. 8(a), which presents a large dark area (about 80000 pixels) due to the large departure. Then the SA-HC algorithm was employed to perform DM optimization control to null the interferogram. Note that, the large tilt of the tested surface would lead that the interferogram not being optimized to approximately null. The residual great tilt fringes make the optimization difficult to work. Thus, a coarse optimization by the SA-HC algorithm was implemented to make sparse

fringe for aligning, and then continue to perform the optimization by the SA-HC algorithm. It was an iterative process in the actual experiment. In this part, to prove the optimization effect, we carried out the experiment with an aligned tested surface.

Figure 8 illustrates the process of SA-HC algorithm implementation. The interferogram variations with the program execution process are all shown in Fig. 8(a). In the first step, the SA algorithm was implemented to reduce the N_p of the dark area in the interferogram to zero, as is shown in Fig. 8(b). In this step, the parameters were set as the same as those in the simulation. The N_p decreased to zero after about 448 s as is shown in Fig. 8(b). In the second step, the SA algorithm continued with the optimization object changing to the rms value of the interferogram, followed by the HC algorithm when the rms value was reduced to 4 λ. The process is shown in Fig. 8(c) and the final rms value was reduced to 0.26 λ. The total time cost was 573 s (about 10 minutes). For comparison, the SPGD algorithm and GA were performed to null the initial interferogram as well. The parameters were set as the same as those in the simulation.

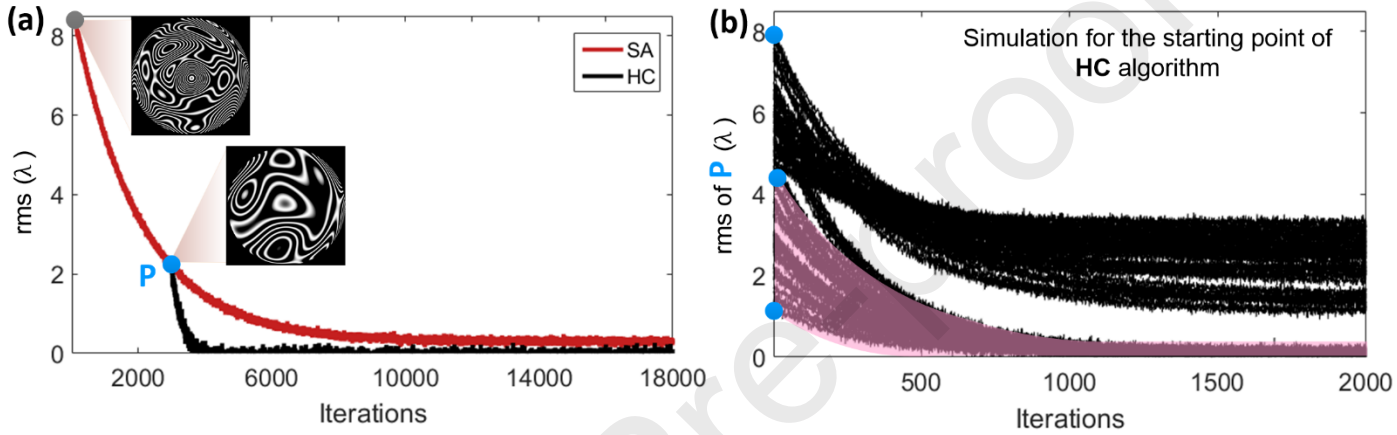

Fig. 6. SA-HC algorithm in the second step. (a) SA-HC algorithm simulation result, (b) Convergence simulation of different initial rms value in the interferogram.

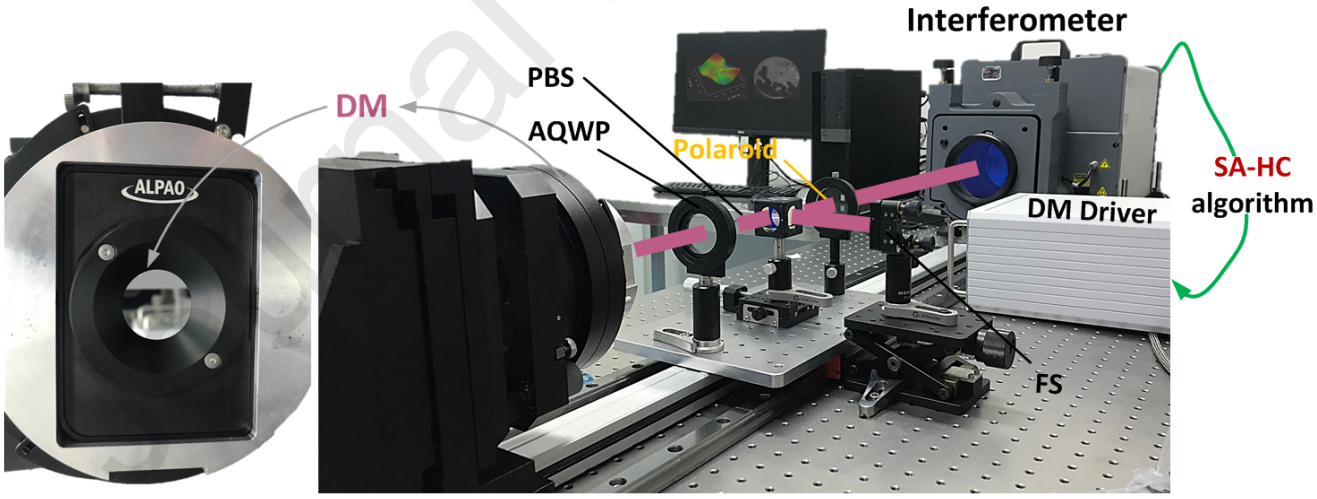

Fig. 7. The experiment system of FSAI.

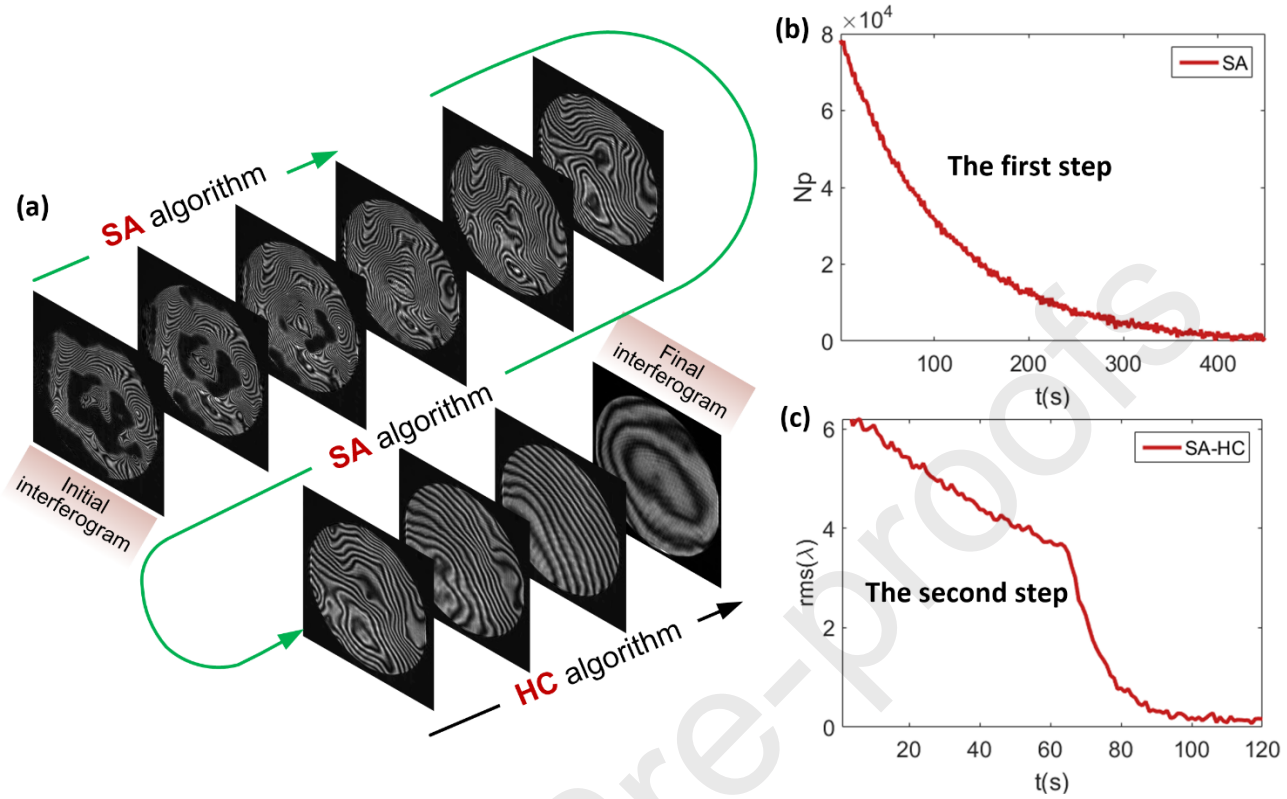

Fig. 8. The process of the SA-HC algorithm implementation. (a) The interferogram variations with the program execution process, (b) Np variations in the first step by the SA algorithm, (c) rms value variations of the interferogram in the second step by SA-HC algorithm.

Figure 9 illustrates the process of SPGD algorithm implementation. In the first step, the SPGD algorithm was implemented to reduce the N_p of dark area in the interferogram to zero as well. The interferogram variations with the program execution process in 1000 s are all shown in Fig. 9(a). The N_p decreased to about 5.8×10^4 after about 181 s and then hold steady as is shown in Fig. 9(b). Figures 9(a) and 9(b) show that the algorithm was trapped in a local minimum. Figure 10 illustrates the process of the GA implementation. The interferogram variations with the program execution process are all shown in Fig. 10(a). In the first step, the GA algorithm was implemented to reduce the N_p of dark area in the interferogram to zero as well, as is shown in Fig. 10(b). The N_p decreased to zero after about 3500 s. In the second step, the GA continued with the optimization objective changing to the rms value of the interferogram. The process is shown in Fig. 8(c) and the final rms value was reduced to 0.57 λ after another 3000s. The total time cost was 6542 s (109 minutes). Figures 8-10 indicate that the SA-HC algorithm in FSAI has a low non-convergence rate while maintaining a relatively high convergence speed. Compared with the previously reported SPGD algorithm and GA, the SA-HC algorithm is more applicable to the test of volume produced in the optical shop.

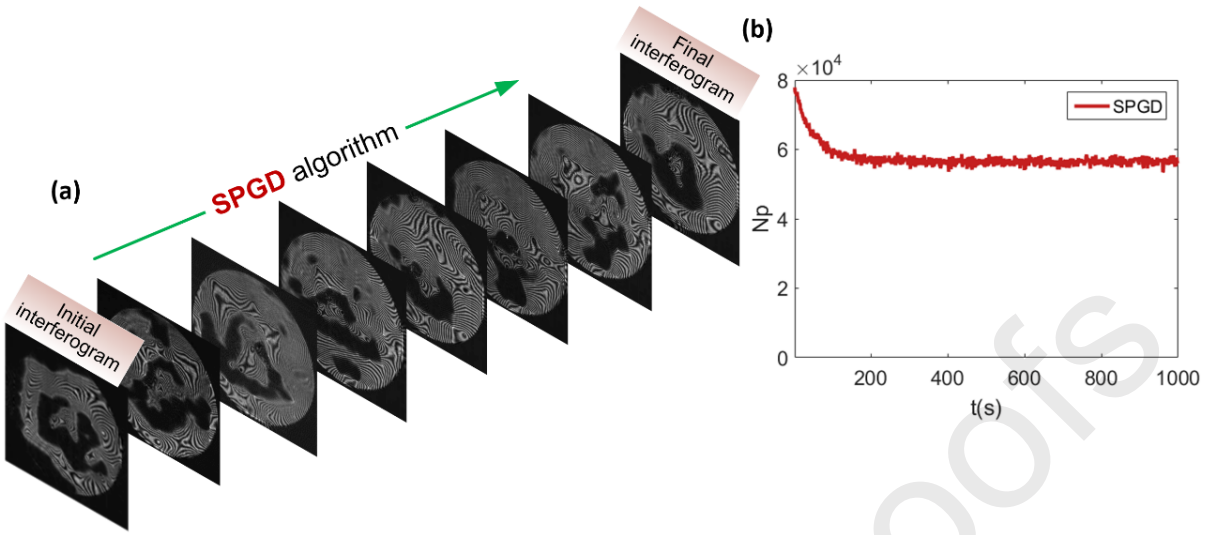

Fig. 9. The process of the SPGD algorithm implementation. (a) The interferogram variations with the program execution process, (b) Np variations in the first step by the SPGD algorithm.

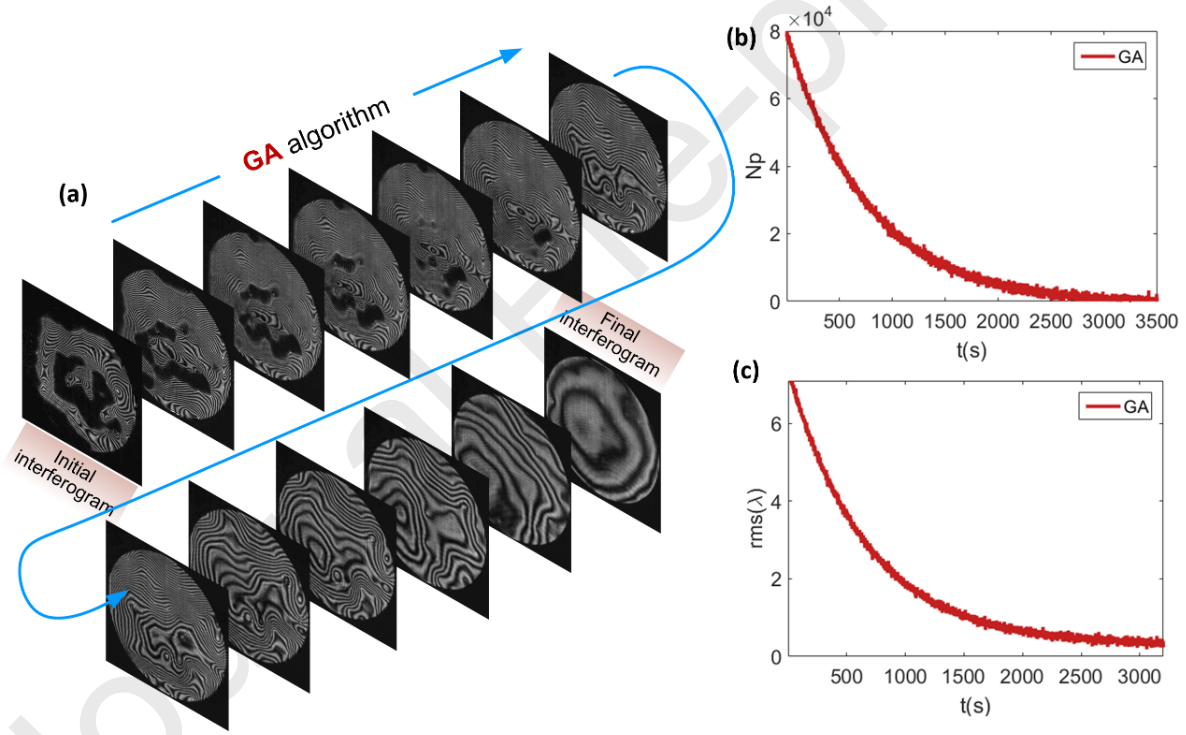

Fig. 10. The process of the GA. (a) The interferogram variations with the program execution process, (b) Np variations in the first step by the GA, (c) rms value variations of the interferogram in the second step by the GA.

As the tested freeform surface, the flat sheet then was pressed randomly to produce various surface shapes to validate the SA-HC algorithm. The initial interferograms are illustrated in Fig. 11(a). The whole measurement process was performed. The final corresponding tested interferograms are illustrated in Fig. 11(b). The DM surface monitoring is performed as is shown in Fig. 1(c) and the results are illustrated in Fig. 11(c). Of course, the DM was calibrated in advance as described in [16]. Then the system model was set up for ray tracing, with the resulting null interferogram (Fig. (b)) and DM monitoring interferogram (Fig. (c)). The freeform surface figure was extracted by the ray-tracing with Zernike polynomials fitting [16, 17]. Measurement results of freeform surface figure maps are illustrated in Fig. 11(d). The average optimization time is about 143 s (2.4 minutes). Meanwhile, the SPGD, SPGD-Newton algorithms, and GA are employed as the comparison. The performance of the corresponding algorithm is listed in Tab. 1. It is proved that the SA-HC algorithm can perform the adaptive metrology of freeform

surfaces with large departures excellently in optical shop testing.

As is shown in Fig. 11, the DM monitoring interferograms have relatively dense fringes than the tested null interferograms. In experiments, there should be a balance in fringe density for them. In fact, it is not necessary to null the final tested interferograms completely. The real optimization criterion is that both interferograms are resolvable in the interferometer. Therefore, the optimization time would be further shortened.

Table 1

The performance comparison of mentioned algorithms

	SA-HC	SPGD	SPGD-Newton	GA
Average Convergence time(minute)	2.38	2.30	1.86	20.45
Convergence Rate(%)	100	83	83	100

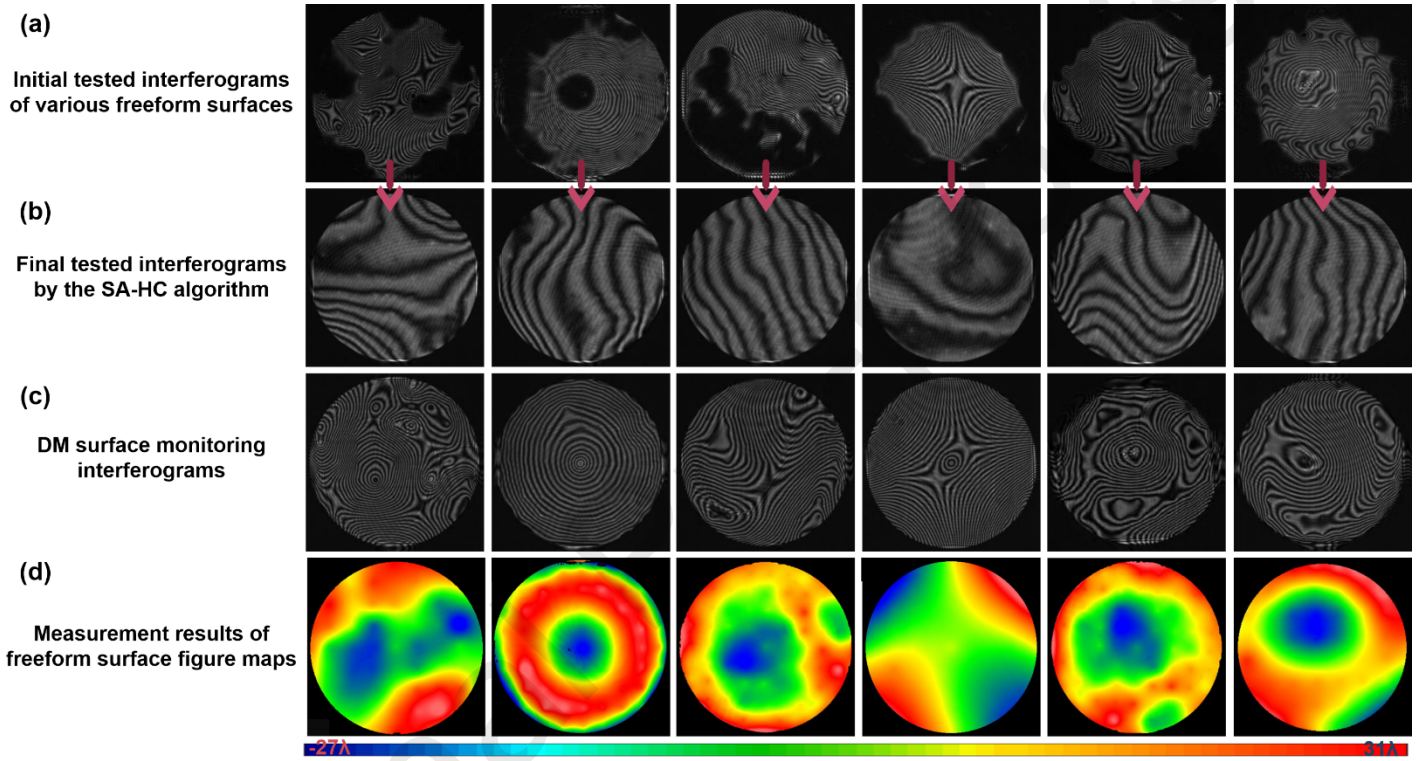

Fig. 11. Measurement results of various freeform surfaces. (a) The initial tested interferograms, (b) The final tested interferograms by the SA-HC algorithm, (c) the DM surface monitoring results, (d) Measurement results of freeform surface figure maps.

6. Conclusion

In the FSAI, the first step in the measurement is nulling the interferogram by the adaptive compensator. Different from the traditional WFL adaptive optical system, the direct optimization object in the FSAI is the interferogram with undistinguished fringes even dark areas. We employed the SA-HC mixed algorithm to perform optimization to release the fringes density and thus to realize a near null test. The optimization is divided into two steps. The first one is to recover full aperture distinguishable fringes by the SA algorithm. The second one is to realize the near null fringes from the dense fringes by the SA and HC algorithms. Simulation and experiment results show that the proposed SA-HC algorithm overcomes the contradiction between the convergence rate and the convergence time. It has a much better convergence rate than the SPGD algorithm, comparable to GA (close to 100%). At the same time, it is much faster than the GA. With an interferogram with no more than a third of a pixel of dark areas, the convergence time of the SA-HC algorithm is approximately 2 minutes (Intel Xeon Scalable 6148 CPU), far less than the 20 minutes of the GA. Therefore, it is applicable to the test of volume produced in the optical shop.

Funding

National Natural Science Foundation of China (61705002, 61905001, 41875158); Natural Science Foundation of Anhui Province (1808085QF198, 1908085QF276); Doctoral Start-up Foundation of the Anhui University (J01003208); National Program on Key Research and Development Project of China (2016YFC0301900, 2016YFC0302202).

Declaration of Competing Interest

The authors declare that they have no known competing financial interests or personal relationships that could have appeared to influence the work reported in this paper.

References

[1] J. Reimers, A. Bauer, K. P. Thompson, J. P. Rolland, Freeform spectrometer enabling increased compactness, *Light-Sci. Appl.* **6**(2017) e17026.

[2] T. Yang, G. Jin, J. Zhu, Automated design of freeform imaging systems, *Light-Sci. Appl.* **6**(2017) e17081.

[3] T. Gissibl, S. Thiele, A. Herkommer, H. Giessen, Sub-micrometre accurate free-form optics by three-dimensional printing on single-mode fibres, *Nat. Commun.* **7**(2016) 11763.

[4] D. Wang, P. Xu, Z. Wu, X. Fu, R. Liang, Simultaneous multi-surface measurement based on computer-aided deflectometry for freeform refractive optics, *Optica* **7**(2020) 1056-1064.

[5] L. Yan, W. Luo, G. Yan, X. Wang, X. Tang, Subaperture stitching testing for fine flat mirrors with large apertures using an orthonormal polynomial fitting algorithm, *Opt. Laser Eng.* **120**(2019) 49-58.

[6] Z. Yang, J. Dou, Q. Yuan, Z. Gao, Lensless phase-shifting point diffraction interferometer for spherical mirror measurement, *Opt. Laser. Eng.* **107**(2018) 119-126.

[7] D. Zhu, F. Wang, P. Li, M. Li, Research on hybrid compensation testing of convex aspherical mirror, *Opt. Laser Eng.* **132**(2020) 106108.

[8] A. Offner, A Null Corrector for Paraboloidal Mirrors, *Appl. Opt.* **2**(1963) 153-155.

[9] W. Fan, Design of dall compensator for aspherical surface null testing., *J. Appl. Opt.*(1993).

[10] J. J. Sullivan, J. E. Greivenkamp, Design of partial nulls for testing of fast aspheric surfaces, *Proc. SPIE* **6671**(2007) 66710W.

[11] J. E. Greivenkamp, R. O. Gappinger, Design of a nonnull interferometer for aspheric wave fronts, *Appl. Opt.* **43**(2004) 5143-5151.

[12] J. C. Wyant, P. K. O'Neill, Computer generated hologram; null lens test of aspheric wavefronts, *Appl. Opt.* **13**(1974) 2762-2765.

[13] Z. Hong, R. Liang, IR-laser assisted additive freeform optics manufacturing, *Sci. Rep.-UK* **7**(2017) 7145.

[14] C. Pruss, H. J. Tiziani, Dynamic null lens for aspheric testing using a membrane mirror, *Opt. Commun* **233**(2004) 15-19.

[15] L. Huang, H. Choi, W. Zhao, L. R. Graves, D. W. Kim, Adaptive interferometric null testing for unknown freeform optics metrology, *Opt. Lett.* **41**(2016) 5539-5542.

[16] L. Zhang, S. Zhou, D. Li, Y. Liu, T. He, B. Yu, J. Li, Pure adaptive interferometer for free form surfaces metrology, *Opt. Express* **26**(2018) 7888-7898.

[17] L. Zhang, S. Zhou, D. Li, J. Li, B. Yu, Model-based adaptive non-null interferometry for freeform surface metrology, *Chin. Opt. Lett.* **16**(2018) 812038.

[18] S. Xue, S. Chen, Z. Fan, D. Zhai, Adaptive wavefront interferometry for unknown free-form surfaces, *Opt. Express* **26**(2018) 21910-21928.

[19] S. Xue, S. Chen, G. Tie, Y. Tian, H. Hu, F. Shi, X. Peng, X. Xiao, Flexible interferometric null testing for concave free-form surfaces using a hybrid refractive and diffractive variable null, *Opt. Lett.* **44**(2019) 2294-2297.

[20] S. Xue, S. Chen, G. Tie, Y. Tian, Adaptive null interferometric test using spatial light modulator for free-form surface, *Opt. Express* **27**(2019) 8414-

8428.
[21] L. Zhang, C. Li, X. Huang, Y. Zhang, S. Zhou, J. Li, B. Yu, Compact adaptive interferometer for unknown freeform surfaces with large departure, *Opt. Express* **28**(2020) 1897-1913.
[22] L. Zhang, Y. Zhang, Freeform surface interferometry with an adaptive ring-cavity compensator, *Surf. Topogr.: Metrol. Prop.* **8**(2020) 25036.
[23] R. Chaudhuri, J. Papa, J. P. Rolland, System design of a single-shot reconfigurable null test using a spatial light modulator for freeform metrology, *Opt. Lett.* **44**(2019) 2000-2003.
[24] H. Song, R. Fraanje, G. Schitter, H. Kroese, G. Vdovin, M. Verhaegen, Model-based aberration correction in a closed-loop wavefront-sensor-less adaptive optics system, *Opt. Express* **18**(2010) 24070-24084.
[25] Q. Yang, J. Zhao, M. Wang, J. Jia, Wavefront sensorless adaptive optics based on the trust region method, *Opt. Lett.* **40**(2015) 1235-1237.
[26] Q. Tian, C. Lu, B. Liu, L. Zhu, X. Pan, Q. Zhang, L. Yang, F. Tian, X. Xin, DNN-based aberration correction in a wavefront sensorless adaptive optics system, *Opt. Express* **27**(2019) 10765-10776.
[27] S. Lohani, R. T. Glasser, Turbulence correction with artificial neural networks, *Opt. Lett.* **43**(2018) 2611-2614.
[28] E. J. Fernández, P. Artal, Membrane deformable mirror for adaptive optics: performance limits in visual optics, *Opt. Express* **11**(2003) 1056-1069.
[29] P. Prieto, E. Fernandez, S. Manzanera, P. Artal, Adaptive optics with a programmable phase modulator: applications in the human eye, *Opt. Express* **12**(2004) 4059-4071.
[30] E. J. Fernández, I. Iglesias, P. Artal, Closed-loop adaptive optics in the human eye, *Opt. Lett.* **26**(2001) 746-748.
[31] 31. S. Xue, W. Deng, S. Chen, Intelligence enhancement of the adaptive wavefront interferometer, *Opt. Express* **8**(2019) 11084-11102.
[32] Y. Zhang, X. Tian, R. Liang, SPGD and Newton iteration mixed algorithm used in freeform surface metrology, *Opt. Laser Eng.* **129**(2020) 106050.
[33] D. Liu, T. Shi, L. Zhang, Y. Yang, S. Chong, Y. Shen, Reverse optimization reconstruction of aspheric figure error in a non-null interferometer, *Appl. Opt.* **53**(2014) 5538-5546.
[34] S. Zommer, E. N. Ribak, S. G. Lipson, J. Adler, Simulated annealing in ocular adaptive optics, *Opt. Lett.* **31**(2006) 939.
[35] L. Ying, J. Ma, B. Li, J. Chu, Hill-climbing algorithm based on Zernike modes for wavefront sensorless adaptive optics, *Opt. Eng.* **52**(2013) 6601.
[36] Z. Fayyaz, N. Mohammadian, F. Salimi, A. Fatima, M. R. R. Tabar, M. R. N. Avanaki, Simulated annealing optimization in wavefront shaping controlled transmission, *Appl. Optics* **57**(2018) 6233-6242.
[37] M. Dai, K. Peng, M. Luo, J. Zhao, W. Wang, Y. Cao, Dynamic phase measuring profilometry for rigid objects based on simulated annealing, *Appl. Opt.* **59**(2020) 389-395.
[38] R. El-Agmy, H. Bulte, A. H. Greenaway, D. Reid, Adaptive beam profile control using a simulated annealing algorithm, *Opt. Express* **13**(2005) 6085-6091.
[39] T. Chaigne, O. K. A. C, A. C. Boccara, M. Fink, E. Bossy, S. Gigan, Controlling light in scattering media non-invasively using the photoacoustic transmission matrix, *Nat. Photonics* **8**(2014) 58-64.
[40] A. Mashaghi, P. Partovi-Azar, T. Jadidi, M. Anvari, S. P. Jand, N. Nafari, Enhanced Autoionization of Water at Phospholipid Interfaces, *J. Phys. Chem. C.* **117**(2012) 510-514.

Lei Zhang： Conceptualization, Methodology, Writing- Reviewing and Editing, Project administration.

Renhu Liu： Writing- Original draft preparation, Software.

Jinling Wu： Data curation, Visualization.

Zhongtao Cheng：Investigation, Software.

Sheng Zhou： Validation.

Jingsong Li: Supervision.

Benli Yu: Resources.

Declaration of interests

The authors declare that they have no known competing financial interests or personal relationships that could have appeared to influence the work reported in this paper.

Highlights

- The interferogram of unknown freeform surface of large departure can be addressed.
- The SA-HC algorithm is employed for intelligent performance in interferometry.
- The test of volume-produced in the optical shop would be realized.

s